Laminar-turbulent transition of a non-Newtonian fluid flow

Krishnan Thota Radhakrishnan, Adithya; Poelma, Christian; van Lier, Jules; Clemens, Francois

DOI
10.1080/00221686.2020.1770876

Publication date
2020

Document Version
Final published version

Published in
Journal of Hydraulic Research

Journal of Hydraulic Research

ISSN: (Print) (Online) Journal homepage: https://www.tandfonline.com/loi/tjhr20

Laminar-turbulent transition of a non-Newtonian fluid flow

Adithya Krishnan Thota Radhakrishnan, Christian Poelma, Jules van Lier & Francois Clemens

To cite this article: Adithya Krishnan Thota Radhakrishnan, Christian Poelma, Jules van Lier & Francois Clemens (2021) Laminar-turbulent transition of a non-Newtonian fluid flow, Journal of Hydraulic Research, 59:2, 235-249, DOI: 10.1080/00221686.2020.1770876

To link to this article: https://doi.org/10.1080/00221686.2020.1770876

IAHR AIRH
Taylor & Francis
Taylor & Francis Group

Journal of Hydraulic Research Vol. 59, No. 2 (2021), pp. 235–249
https://doi.org/10.1080/00221686.2020.1770876

Research paper

Laminar-turbulent transition of a non-Newtonian fluid flow

ADITHYA KRISHNAN THOTA RADHAKRISHNAN, PhD Student, *Faculty of Civil Engineering and Geosciences, Delft University of Technology, Delft, the Netherlands*
Email: a.k.thotaradhakrishnan@tudelft.nl (author for correspondence)

CHRISTIAN POELMA, Professor, *Faculty of Mechanical, Maritime and Materials Engineering, Delft University of Technology, Delft, the Netherlands*
Email: c.poelma@tudelft.nl

JULES VAN LIER, Professor, *Faculty of Civil Engineering and Geosciences, Delft University of Technology, Delft, the Netherlands*
Email: j.b.vanlier@tudelft.nl

FRANCOIS CLEMENS, *Faculty of Civil Engineering and Geosciences, Delft University of Technology, Delft, the Netherlands*
Email: f.h.l.r.clemens@tudelft.nl

ABSTRACT
Transition from laminar to turbulent flow of non-Newtonian fluids is investigated using velocimetry data. These data are obtained by applying particle image velocimetry to images obtained through ultrasound imaging (echography). This yielded the observation of intermittent structures (puffs and slugs) that are formed during transition. Post its observation, transition is characterized using the friction factor curves and turbulence intensity. Further, a number of models used to predict transition are assessed. This showed the Reynolds number based model by Slatter and the stability parameter based model by Hanks to be most suitable for non-Newtonian fluids with yield stress and low behaviour index.

Keywords: Intermittent structures; non-Newtonian; PIV; transition; ultrasound

1 Introduction

Flows of non-Newtonian fluids or slurries are commonly found in a variety of process systems. The flow of slurries in wastewater treatment plants is a commonly encountered example. Characterizing their flow regime is an important factor in the overall hydraulic design and the operation of the equipment handling them. Predicting the flow regime as laminar, transitional or turbulent has been a major part of the study on non-Newtonian flows in the recent decades. As the gap between theoretical understanding and experimental findings of Newtonian fluids closes, non-Newtonian fluids are starting to become a new realm of fluids waiting to be explored, with transition in their flow forming a fundamental importance. Studying the transition of flow from laminar to turbulent has two aspects to it : (1) identifying the conditions under which transitions occurs and (2) the possibility of predicting these transitions. Both are discussed in the following sections.

1.1 *Characterizing transition*

Transition from laminar to turbulent flow is known to occur through intermittent flow structures which evolve from disturbances in the flow. A number of classic experimental works on Newtonian fluids (Darbyshire & Mullin, 1995; Lindgren, 1969; Nishi et al., 2008; Wygnanski et al., 1975; Wygnanski & Champagne, 1973) and non-Newtonian fluids (Draad et al., 1998; Güzel, Burghelea, et al., 2009) have focused on studying the transitional regime and have shown that two distinct flow structures exist: puffs and slugs. The occurrence of these structures depends on the Reynolds number ($\mathrm{Re} = DV\rho/\mu$); puffs occur at relatively low Reynolds numbers and slugs at a higher Reynolds numbers. Although the transition information on non-Newtonian fluids is very limited, a great amount of information is obtained for Newtonian fluids, through the experimental studies performed in circular pipes that have already been mentioned, it is seen that

Received 15 April 2019; accepted 10 May 2020/Open for discussion until 1 November 2021.

ISSN 0022-1686 print/ISSN 1814-2079 online
http://www.tandfonline.com

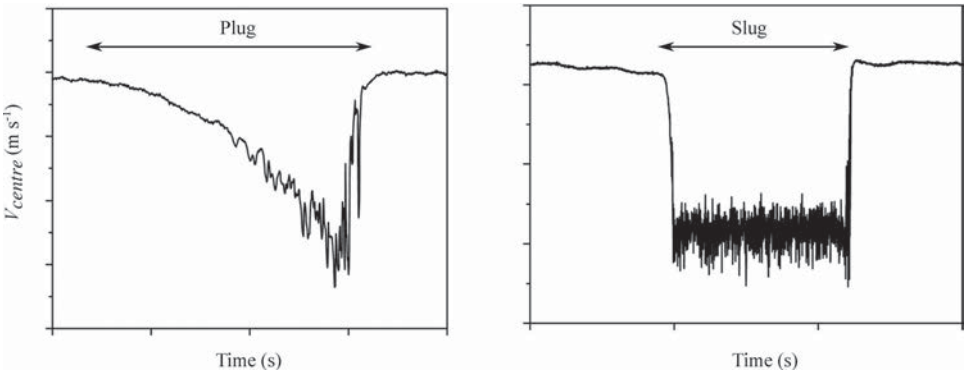

Figure 1 Velocity trace (adopted from Nishi et al., 2008) at the centre of the pipe showing the presence of puff (left) and slug (right)

puffs are found when $\mathsf{R_e} \lessapprox 2700$ and slugs are found when $\mathsf{R_e} \gtrapprox 3000$.

To characterize puffs and slugs, changes in the local velocity are often used. Puffs are identified as having a saw-toothed velocity trace (gradually decreasing, followed by a more sudden jump back to the undisturbed velocity); see e.g. Nishi et al. (2008) and Wygnanski and Champagne (1973). These puffs represent isolated patches of turbulent flow and are dissipated downstream along the flow (Fig. 1, left). On the other hand, the velocity trace of the slugs is identified as having a square shape (Fig. 1, right), with properties similar to that of fully developed turbulence within them (Nishi et al., 2008). Its leading edge is found to travel faster than the average flow velocity and its trailing edge, thereby increasing in length as it travels downstream.

1.2 *Predicting transition*

For Newtonian fluids, transition can be predicted in practical applications based on the well-established critical Reynolds number (2100–2300 for pipe flows). Although $\mathsf{R_e} = 2300$ is usually referred as the critical Reynolds number for transition to turbulence, under controlled conditions, the laminar pipe flow can be maintained for much higher Reynolds number (Hof et al., 2003). There is a wide range of theories and models available to predict this onset of transition (Avila et al., 2011; Eckhardt et al., 2007), and such a range is due to the difficulty that transition as a phenomenon is not very well defined and occurs over a range of Reynolds numbers (Darbyshire & Mullin, 1995; Draad et al., 1998). For non-Newtonian fluids, a complicating factor is the representation of the fluid behaviour in simple rheological models. The commonly used rheological models are the power-law and the Herschel–Bulkley model (Thota Radhakrishnan et al., 2018), which will also form a basis for this study. The shear-stress and shear-rate are related using the power function $\tau = K\dot{\gamma}^n$ in a power-law model, where K is the fluid consistency index and n is the behaviour index. The behaviour index n is called so as it suitably represents the behaviour of the fluid as shear-thinning for $n < 1$, Newtonian for $n = 1$ and shear-thickening for $n > 1$. For this study n takes the values $0 < n \leq 1$. As for the Herschel–Bulkley model, it is represented as $\tau = \tau_y + K\dot{\gamma}^n$. The yield-stress τ_y is the minimum shear-stress that is required for a fluid (of the Herschel–Bulkley type) to deform. The presence of a yield stress in a fluid produces a plug-like structure at the centre of the pipe in laminar flow, and deteriorates at turbulent flow (Güzel, Frigaard, et al., 2009). At transition, the flow may be affected by the yield stress. The rheological models are only a simplified representation of a small set of measured quantities, i.e. measuring only the shear-stress vs. shear-rate while ignoring other information – such as the type of fluid (e.g. thixotropy) and the particles involved (in the case of a slurry). As a consequence, the Reynolds number is no longer defined in a trivial manner, as there is no longer a single value that represent the viscosity. Nevertheless, there is a need for models that predict/describe the transition in non-Newtonian fluids/slurries. The ones most commonly referred to in the literature are described below. These models can be categorized as either Reynolds number based or stability parameter-based models.

Reynolds number based

Hedstrom (1952) proposed the intersection method wherein the transition is defined as to occur at the Reynolds number associated with the intersection of the (extrapolated) laminar and turbulent friction factor curves. Although simple, the result is highly dependent on the choice and accuracy of the turbulent model (friction factor curves, e.g. Blasius friction curve) and is regarded as an ambiguous criterion.

Metzner and Reed (1955) analysed data from a series of pipe flow experiments of different non-Newtonian fluids and pointed out that the flow curves deviated from the laminar flow curve at approximately the same Reynolds number $\mathsf{R_e}$ as Newtonian fluids. Considering the Fanning friction factor ($f = R\Delta P/\rho LV^2$) as a stability parameter, they proposed that transition would take place at $f \approx 0.0076$. To calculate the friction factor, the Metzner–Reed Reynolds number $\mathsf{R_{eMR}}$ (Eq. 1) is used, and at transition it corresponds to a value of ≈ 2100. The parameters in Eq. (1) are derived as n representing the slope of a logarithmic plot of $D\Delta P/4L$ versus $8V/D$, which was found to be nearly constant for most non-Newtonian fluids investigated by

the authors over a wide range of shear stresses. K' is the coefficient from the integration of the expression representing the wall shear rate as a function of the pressure drop and the volumetric flow rate, which finally leads to $D\Delta P/4L = K'(8V/D)^{n'}$. The $\mathsf{Re}_{\mathsf{MR}}$ is based on power-law fluids; for Herschel–Bulkley fluids the parameters in $\mathsf{Re}_{\mathsf{MR}}$ are dependent on the yield stress, which imposes complications:

$$\mathsf{Re}_{\mathsf{MR}} = \frac{8V^2\rho}{K'(\frac{8V}{D})^n}, \quad K' = K\left(\frac{1+3n}{4n}\right)^n \tag{1}$$

Slatter (1995) proposed a Reynolds number (Eq. 2) accounting for a solid plug at the centre of the pipe flow due to the presence of yield stress in the fluid. For the Reynolds number, transition is considered to occur at a value of 2100. The unsheared plug at the centre is treated as a solid plug and its flow is subtracted from the mean fluid flow to determine the effective flow velocity of the annular, sheared region (Eq. 3):

$$\mathsf{Re}_{\mathsf{S}} = \frac{8\rho V_{ann}^2}{\tau_y + K(8V_{ann}/D_{shear})^n} \tag{2}$$

$$V_{ann} = \frac{Q_{ann}}{A_{ann}} = \frac{Q - Q_{plug}}{\pi(R^2 - R_{plug}^2)} \tag{3}$$

For determining the volumetric flow rate in the plug Eq. (4) is used, which is obtained by integrating the constituent rheological equation, where the radius of the plug is determined using Eq. (5):

$$Q_{plug} = A_{plug}\frac{D}{2K^{(1/n)}\tau_w}\frac{n}{n+1}[(\tau_w - \tau_y)^{(n+1)/n}] \tag{4}$$

$$R_{plug} = \frac{\tau_y}{\tau_w}R \tag{5}$$

Among the Reynolds number-based models, the ones by Slatter and Metzner–Reed will be considered for this study. A brief study by Eshtiaghi et al. (2012) on transition in the flow of non-Newtonian sludge also considered the Slatter and Metzner–Reed models, and concluded that the Slatter model performed better. The Hedstrom method is not considered, since an assumption must be made on the turbulence flow model which is not in the scope of the study. Nevertheless, the Hedstrom method will be used as a verification step, to validate the identified transition through the measured pressure drop.

Stability parameter based

Ryan and Johnson (1959) approached transition through a local stability parameter on the balance of stabilizing and destabilizing forces. The stability parameter is based on the energy-dissipation of disturbances, where the energy exchanges are represented as shear stresses. This stability parameter represented as Z_{RJ} is a function of the ratio of input energy to energy dissipation for a fluid element as shown in Eq. (6). Transition occurs at the boundary between stable laminar and stable turbulent pipe flow, where the stability is considered with respect to the average local velocity (i.e. the time derivative of the local average velocity is zero). At this boundary the stability parameter reaches a critical point represented as $\partial Z_{RJ}/\partial y = 0$ and Z_{RJ} takes the value 808, which is set to be the predictive criterion. This value was derived through the transition of Newtonian fluids and assumed by the authors to be true for all fluid types.

$$Z_{RJ} = \frac{r\rho v_z}{\tau_w}\frac{\partial v_z}{\partial y}, \quad at\frac{\partial Z_{RJ}}{\partial y} = 0 \tag{6}$$

Hanks and co-workers (Hanks, 1963, 1969; Hanks & Dadia, 1971; Hanks & Ricks, 1974) derived a similar criterion to Ryan and Johnson (1959), but for non-Newtonian fluids, through the perspective of angular momentum transfer. The proposed stability criterion is seen to represent the coupling ratio between the rate of change of angular momentum of a deforming fluid element and its rate of momentum loss by frictional drag. At transition, the fluid element is seen to become unstable to rotational disturbance and thus giving rise to turbulent eddies through the nonlinearity of the momentum transfer process. The critical value of the stability parameter was determined to be 404, exactly half of that derived by Ryan and Johnson (1959). Equation (7) represents the derived stability criterion, where $\boldsymbol{w} = \nabla \times \boldsymbol{v}$ is the vorticity vector from the velocity vector $\boldsymbol{v}$ and $\nabla.\,\boldsymbol{\tau}$ is the divergence of the deviatoric stress tensor. For a rectilinear pipe flow, Eq. (7) reduces to Eq. (8). This is derived using the Fanning friction factor to represent the average flow velocity in terms of the rheological model. In practice, Eq. (8) is used, setting $Z_H = 404$, to derive the transition critical flow velocity:

$$Z_H = |\rho\boldsymbol{v} \times \boldsymbol{w}|/|\nabla.\boldsymbol{\tau}| \tag{7}$$

$$Z_H = \frac{\mathsf{Re}}{16}\left(\frac{v}{V}\right)\left(-\frac{d(v/V)}{d(r/r_w)}\right) \tag{8}$$

Mishra and Tripathi (1971) pointed out that transition occurs through a stepwise process. The consecutive steps are described as follows: two-dimensional waves, three dimensional waves, a turbulent spot and propagation of the turbulent spot to the entire field. The formation of the turbulent spot coincides with the point where the rate of change of the mean velocity is at its maximum. With this, they accordingly proposed that the average kinetic energy per unit volume in the fluid and the shear stress at the wall to be the important factors governing the transition. Through this they derived a stability parameter as the ratio of the kinetic energy per unit volume of the fluid and the wall shear stress and also postulate that it should remain the same for all purely viscous non-Newtonian fluids.

Among the stability parameter-based models the one of Hanks and co-workers will be considered for this study. This is because all the models are very similar at the implementation, and only the theory behind the model development is different. Also, the Hanks model is very well documented for

the use of Herschel–Bulkley fluids (being the main rheological model considered in this study) while the other two are not well documented and pose difficulties in their implementation for Herschel–Bulkley fluids.

It is not claimed that the previous discussion encompasses a complete list of the predictive methods that have been proposed. Some that have not been mentioned are either modifications or extensions of the ones discussed. Readers interested in these are referred to the literature (e.g. Güzel, Burghelea, et al., 2009).

Studying and examining laminar turbulent transition in the flow of fluids including non-Newtonian fluids have been made possible through many experimental techniques. These techniques include hot wire anemometry (Nishi et al., 2008; Wygnanski & Champagne, 1973), laser Doppler anemometry/velocimetry (Draad et al., 1998; Escudier & Presti, 1996; Güzel, Burghelea, et al., 2009; Peixinho et al., 2005), stereoscopic PIV (Van Doorne & Westerweel, 2007) and more recently ultrasound imaging velocimetry (UIV) (Hogendoorn & Poelma, 2018). The choice of the experimental technique in most cases certainly depends on the test fluid properties and the capability to be intrusive. In the case of hot-wire anemometry and laser Doppler anemometry, the information of the flow obtained is a time series at a particular point in the flow. Meanwhile, the UIV technique gives information about the flow field within a time range. This technique is both non-invasive and applicable to optically inaccessible fluids. The work of Hogendoorn and Poelma (2018) states the applicability of using UIV as a technique to acquire flow fields of fluids with particles and observe transition in them. Given the applicability of the UIV technique, this will be used in this study.

This study aims to investigate laminar-turbulent transition and verify models that predict this transition in non-Newtonian fluids. The main outline of the paper is as follows. A flow loop is built to achieve fully-developed steady state flows of non-Newtonian fluid in a circular pipe; the set-up is detailed in Section 2. Using this set-up, the pressure drop along the pipe is measured at various flow rates for different concentrations of a non-Newtonian slurry. Along with this the instantaneous velocity field is quantified to investigate laminar-turbulent transition using UIV (Section 3.3). It must be noted that the dataset obtained is both unique, considering such a large flow loop, and novel when taking into account the UIV method applied. The velocimetry data will be used to identify and investigate the formation of intermittent fluid structures present during transition and identify transition. Considering the availability of many predictive model candidates (Section 1.2), the aim of this paper is to verify the available predicting methods for transition in non-Newtonian fluids.

2 Experimental set-up

All the measurements of pressure drop and UIV data reported in this study were performed in a 200 m long closed-loop recirculation pipeline system with an inner diameter of 100 mm. The set-up is schematically represented in Fig. 2. A variable frequency centrifugal slurry pump is used to maintain the flow of the slurry. The desired flow rate is achieved by setting an appropriate outlet pressure or pump rotor rotation frequency. A slurry tank of approximately 4 m^3 capacity upstream of the pump contains the slurry for the measurements. The slurry tank, with two outlets at the bottom and two inlets at the top, is capable of generating a vortex when a cross inflow-outflow to the tank is selected. This vortex is instrumental in keeping the slurry continuously mixed in order to obtain a constant composition of the slurry. To aid the mixing, a submersible pump is fitted inside at the bottom of the tank opposite the outlets to further stimulate the mixing process.

To ensure a completely developed velocity profile at the test sections, the entry and exit lengths from the test sections are to be considered. The minimum requirement that is to be satisfied is that of the laminar flow, as it is known the entry length for a turbulent flow is shorter than that of a laminar flow (Bewersdorff & Thiel, 1993; Bogue, 1959; Chen, 1973; Froishteter

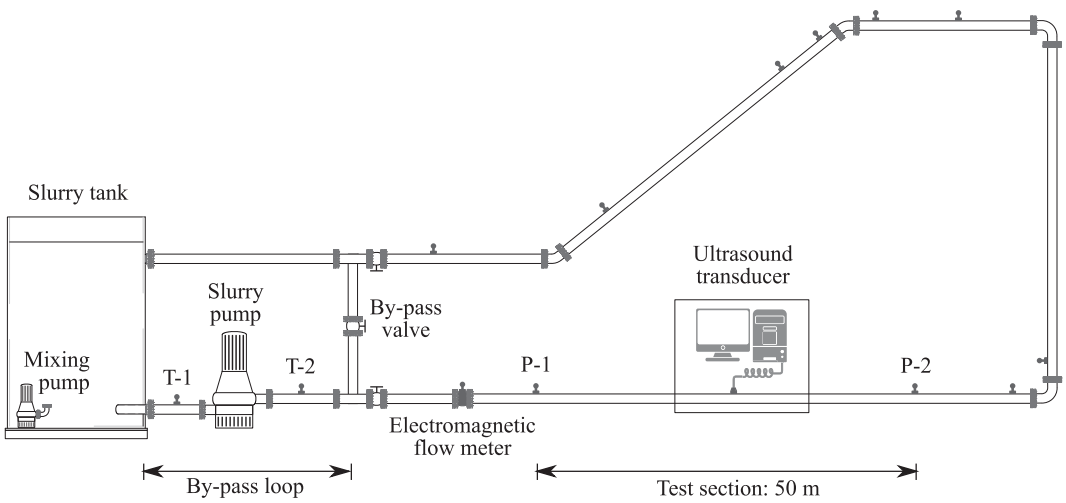

Figure 2 Schematic representation of the experimental set-up. T-1, T-2: temperature sensors, P-1, P-2: pressure sensors

& Vinogradov, 1980; Soto & Shah, 1976). The entry length L_e/D is widely accepted to scale with $\mathrm{R_e}/30$ (Durst et al., 2005; Poole & Ridley, 2007). Therefore, for the case of transition at around $\mathrm{R_e} = 2300$ the acceptable entry length would be around 75 pipe diameters. The test section made of PVC is downstream of the pump and has a length of 50 m (length to diameter ratio: 500). The pressure drop across the test section is measured using a pressure transducer placed at either ends of the pipe. To ensure complete developed flow the test section has an entrance length of 20 m (length to diameter ratio: 200) and an exit length of 15 m (length to diameter ratio: 150). This exceeds the standard prescribed entrance and exit lengths.

The pressure drop across the test section is measured using two submersible pressure transducers P-1 and P-2 (PDCR5031, GE) placed at either ends of the test section. These contain a micro-machined silicon piezo resistive pressure sensor which provides a linearized output voltage proportional to the pressure measured with an accuracy of 0.04% over its full scale. The temperature of the flowing slurry is measured before and after the pump using a temperature sensor (STS-PT100, Ametek, Berwyn, Pennsylvania, USA) with an accuracy of 0.04%. The average volumetric flow rate is measured using an electromagnetic flow meter (Optiflux 2300C, KROHNE Nederland B.V., Dordrecht, Netherlands) which is placed 10 m upstream of the test section. The data from these sensors are recorded at the rate of 1 kHz. For obtaining the UIV data the ultrasound transducer is placed at the centre of the test section (more details of the UIV system are given in Section 3.3).

3 Materials and methods

3.1 *Test fluid*

The slurry that is used in this experiment is based on kaolin clay, of the type used for making ceramics. The slurry is formed through the suspension of the clay particles in water. The particle size distribution of the particulates suspended in water is examined using Microtrac Bluewave diffraction analyser (Malvern Instruments Ltd, Malvern, UK) equipped with Microtrac FLEX 11 Software and is given in Fig. 3a. These suspended particulates are in the range of 5–55 µm and have a d_{85} of 38 µfu (d_{85} is a representative diameter of the suspended particles, where 85% of the particles are below this diameter). For most of the work the shear dependence of the slurry is considered to dominate other fluid behaviour like visco-elasticity and thixotropy. The shear dependence is modelled using a Herschel–Bulkley rheology model (Masalova et al., 2006; Slatter, 1995). The rheology of the slurry (Table 1, Fig. 3b) was obtained using a rotational rheometer. An MCR302 instrument from Anton Paar, equipped with a standard cup and bob (cup diameter: 29.29 mm, bob diameter: 27 mm, bob length: 40.5 mm), was used for this purpose. The selected shear-rate range for the measurement of the rheogram is important as this is known to influence the representative rheology of the slurry, which will be used to further estimate the turbulent pressure losses (Singh et al., 2016). The selection of the shear-rate range is chosen considering the importance of low shear-rates for representing laminar flow and transition accurately, and also considering the onset of secondary flows at higher shear-rates. As the rheology is dependent on temperature, a Peltier temperature control system was used to set and maintain the temperature with an accuracy of $\pm 0.1^{\circ}$C. The concentration and temperature of the different slurry samples are the same as the one used in the loop experiment. The slurry's non-Newtonian behaviour is dependent on the concentration of solids, as can be seen from Table 1 and Fig. 3b; at low concentrations the slurry is typically a power law fluid and at high concentrations it behaves as a Herschel–Bulkley fluid: it has a non-zero yield stress. The parameters of the rheological model shown in Table 1 are estimated using a golden section search algorithm (Thota Radhakrishnan et al., 2018) to address the estimation of the yield stress. This algorithm has been found to estimate the yield stress very well (Kelessidis et al., 2006).

3.2 *Experimental procedure*

The system was initially filled with water and the pressure drop across the test section was measured at various flow rates. For

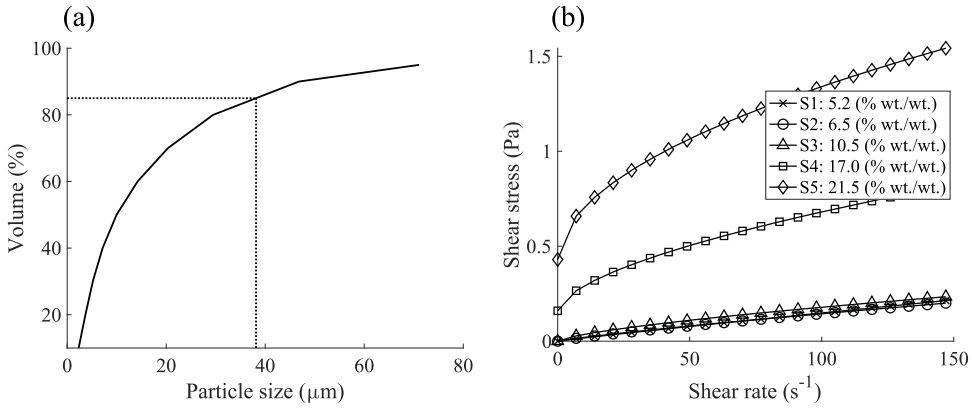

Figure 3 (a) Cumulative particle size distribution of suspended slurry particulates in water, with a d_{85} of 38 µm. (b) Slurry rheology at different concentrations. (For the sake of representation, only a few points are plotted here, instead of the full dataset)

Table 1 Slurry characteristics: rheology (Fig. 3b)

Slurry	Concentration (% TSS wt/wt)	Yield Stress: τ_y (Pa)	Consistency index: K (mPa s^n)	Behaviour index: n (–)	Density: ρ (kg m^3)
S1	5.2	0	1.96	0.94	1029
S2	6.5	0	2.88	0.85	1039
S3	10.5	0	7.11	0.70	1067
S4	17.0	0.16	32.84	0.60	1113
S5	21.5	0.43	83.04	0.52	1146

measurements at different concentrations of slurry (S1 to S5, Table 1), a known amount of clay powder was added to the tank and mixed *in situ*. The initial mixing was done through a shorter section (Fig. 2, by-pass loop) of the pipeline by means of a by-pass valve for 3–4 h and then through the entire flow loop for another 3–4 h. During both the mixing and measurements, the small circulation pump and vortex inside the tank ensures complete mixing inside the tank. Slurry samples are taken both during mixing and measurements to determine the slurry concentration and its rheology. During each measurement cycle, the temperature of the slurry varied less than 0.5°C. This recorded temperature of the slurry was also used to set the temperature of the slurry during its rheological measurements.

For each concentration, the measurements of flow pressure drop and velocity profile were measured for different flow rates (bulk flow velocity of 0.64, 0.53, 0.42, 0.32, 0.21 m s^{-1}). The desired flow rate was set by choosing the appropriate outlet pressure and pump rotor frequency. In post-processing, the recorded pressure, temperature and flow rate data was averaged over 200 s.

3.3 *UIV system*

UIV (for details see Poelma, 2017) was used to obtain the velocimetry data for studying the transition in slurry flow. The system consists of an ultrasound imaging module and particle image velocimetry (PIV) processing software. The imaging module was an Ultrasonix SonixTOUCH research system (Analogic Ultrasound, Peabody, Massachusetts, USA) with a linear transducer (L14-5/38 mm aperture). The transducer centred to operate at a frequency of 10 MHz has a linear array of 128 piezoelectric elements and was positioned at the centre of the pipe test section aligned length wise on the outer upper wall (Fig. 4). Aquasonic 100 (Parker Laboratories, Fairfield, NJ, USA) gel was used to couple the transducer to the pipe wall. The radio frequency signals reflected from the flowing slurry are sampled at a rate of 40 MHz and stored in raw format for analysis. With the system set to run in research mode, this allows control to set the specifications of the ultrasound image acquisition parameters. The raw imaging data were acquired over 7–8 s at a frame rate of 400 frames per second. This high frame rate was obtained by setting the system to operate only with 64 elements (or 50% sector) of the transducer and limiting the image depth to 2.5 cm from the upper outer wall of the pipe. The maximum flow velocity of the experiments was limited by the maximum detectable particle displacement for the UIV method.

Custom PIV software (details can be found in Poelma et al., 2012) was used to obtain the velocimetry data from the ultrasound images. Cross-correlation was employed between consecutive images to determine the local particle displacement. A pre-defined interrogation window was chosen in the image pairs and a correlation peak was determined. The location of this correlation peak provides the direction and displacement; this results in a single flow velocity vector. Applying this over the entire image and consecutive image pairs over the recorded data gives a time-series of 2-D velocity profile at the centre-plane of the pipe. Outliers in the velocity field were detected using a median test. These outliers were replaced using an interpolation of the neighbouring vectors. Note: This 2-D time series velocity profile extends only 2.5 cm in depth (being 50% of the pipe's radius) into the pipe from the outer upper pipe wall.

4 Results and discussion

This section has four parts: first, the obtained UIV data are discussed. Next, Using the UIV data the observed transition is characterized. Subsequently, statistical methods are applied to

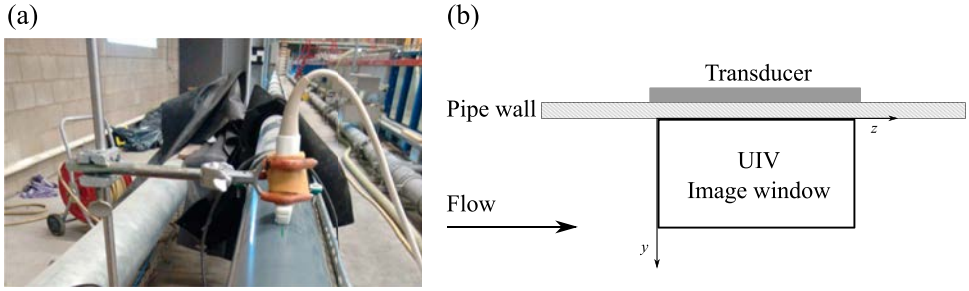

Figure 4 (a) Ultrasound imaging transducer aligned streamwise along the pipe. (b) Schematic representation of the coordinate system on the test section for UIV measurement

the UIV to characterize transition. Lastly, the models that are used to predict transition (Section 1.2) are verified.

4.1 *Ultrasound imaging velocimetry*

Ultrasound images were obtained at 400 Hz over an interval of around 7 s. For each experiment, five sets of data were obtained to ensure statistical convergence. Applying the PIV cross-correlation method mentioned in Section 3.3 to the time-series sequence of the images, a 2D velocity vector field is obtained for each case. Figure 5 shows a typical flow field obtained using the above-mentioned method. The figure shows unidirectional flow with both the presence of wall and the slurry flow regions. The velocity vectors at the wall are due to non-stationary echoes that are common for PVC pipes. For analysis (in the following sections), only the velocity vector field in the slurry flow region is considered.

4.2 *Observing transition*

The resulting vector fields obtained from the PIV (Section 4.1) processing were used to identify the occurrence of flow regime transition. Transition is visualized by plotting a single array of the velocity vectors along the radial direction as a function of time. The plane chosen for these velocity vectors is along the centre of the ultrasound images. This visualization illustrates an evolution of the transition characteristics, i.e. slugs and puffs. A median filter is applied on the velocimetry data to replace the outliers present in the data. As the large-scale structures dominate, the median filter will not hinder the analysis. As a representative case, the different flow velocities of slurry S4 is illustrated in Figs 6 and 7 and these representative cases will form the core of the discussion that follows. Other datasets for the same conditions, as well as the other cases, showed similar behaviour and we focus here on these exemplary datasets. The data for the other cases are available in the supplementary material provided. In Fig. 6, the radial component of the

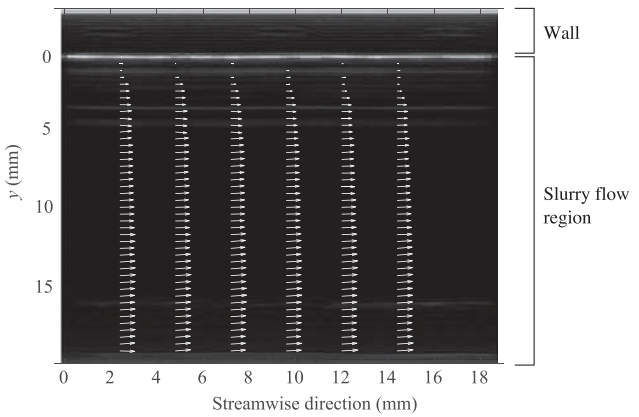

Figure 5 Flow field of the slurry in the pipe derived from UIV. The velocity vectors in the wall region are due to non-stationary echoes, which are discarded and the vectors in the slurry flow region are used for analysis. This is for slurry S1 at average flow velocity of 0.21 m s^{-1}

velocity vector is plotted and in Fig. 7, the axial component (streamwise direction) of the velocity vector is plotted. Using Taylor's hypothesis, the time-series can be interpreted as a spatial sequence (although it is stressed that the image does not represent a true instantaneous snapshot) of the evolution of the structures.

An initial observation of Figs 6 and 7 show the presence of intermittent structures (Figs 6c, d and 7c, d). For further analysis of the intermittent structures, the mean of the velocity components along the radial direction is plotted against time (Fig. 8). The centre line velocity trace is generally used in characterizing these intermittent structures, but due to the limitation of the depth of the flow field in study (i.e. inability to obtain the centreline velocity), the mean of the velocity components that encompasses all the radial positions is used. The plot of the mean also provides an appropriate indication of the intermittent structures, as they are able to indicate deviations from the mean flow (Fig. 8). Analysing the mean plot (Fig. 8), it can be seen that the intermittent structures are similar to the ones observed in previous studies (Nishi et al., 2008; Wygnanski & Champagne, 1973). These intermittent structures are caused by localized perturbations. They induce turbulence at localized sections of the pipe as puffs and slugs. The length of these structures are found to be about 5 pipe diameters (0.5 m) for puffs and 10 diameters (1.0 m) for slugs. This size is particularly low compared to lengths of 30 pipe diameters reported in earlier studies using Newtonian fluids (Eckhardt et al., 2007; Wygnanski & Champagne, 1973). Güzel, Burghelea, et al. (2009) reports that the puff length for Newtonian fluids are approximately 86 pipe diameters, for power-law fluids are in the range of 47–52 pipe diameters and for Herschel–Bulkley fluids approximately 30 pipe diameters, thereby showing that the puff lengths are longer for Newtonian fluids than for non-Newtonian fluids. Figure 8c and h show the presence of structures that appear gradual and dissipate. These structures are characterized as puffs. Figure 8d and i show the presence of slugs which appear as a sharp deviation from the mean flow and persist for a short period of time and then sharply deteriorate. It is also noted that within the structure of slugs, characteristics similar to turbulence can be seen. These intermittent structures could also be observed in the plots of Figs 6 and 7.

Through the occurrence of the intermittent structures, it is identified that transition does not occur at a single stage, as it rather occurs over a range of velocities with different characteristics. The state-of-the-art characterization of transition is through puffs and slugs as already mentioned in Section 1.1. In this study, different stages of transition are identified, based on a combination of the occurrence of puffs and slugs. Figures 6 and 7 (combined with the information from the figures provided as supplementary) show these stages through the time evolution plots of the velocity component. As not all the measured cases undergo all the transition stages, readers are referred to also consider the figures provided as supplementary material. It is observed that the first stage of transition can be identified

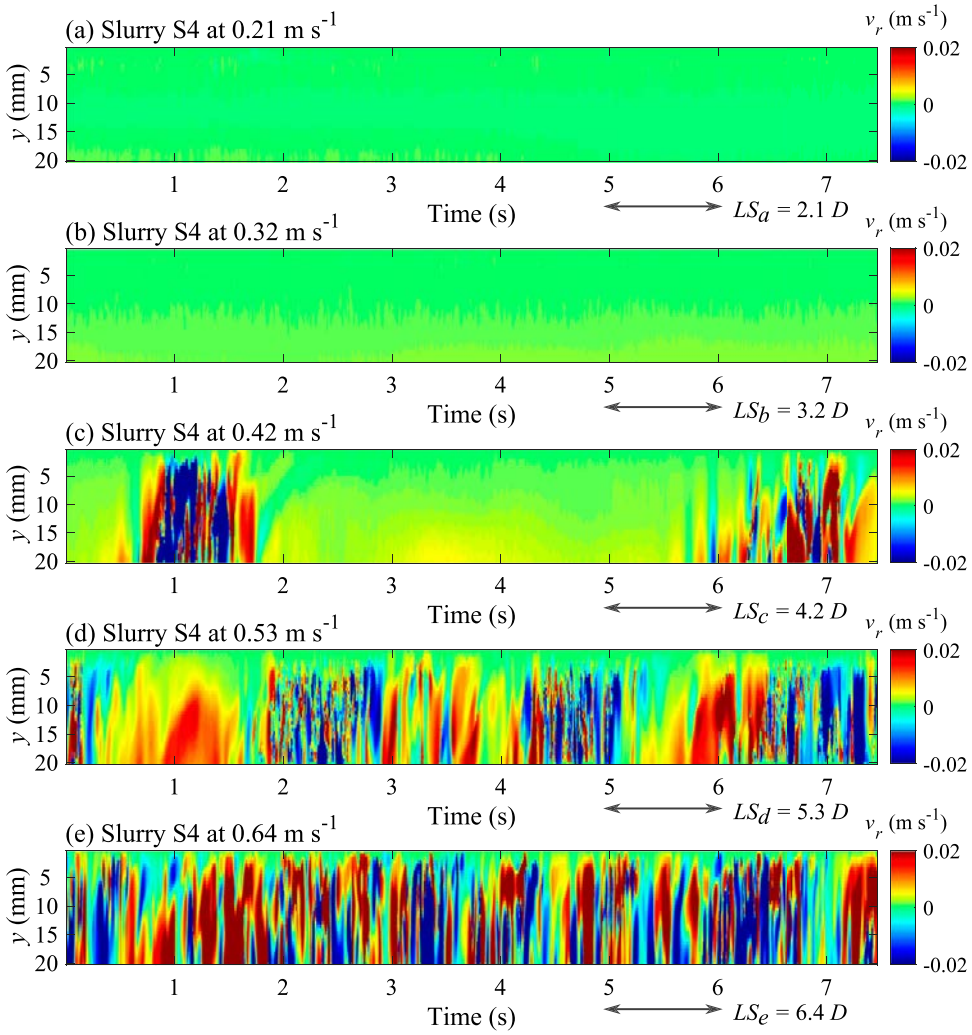

Figure 6 Observing transition through the ultrasound velocimetry data. Plot of the radial component of the velocity vector against time as an estimate for the cross-sectional plane for slurry S4. The length scale (LS) with respect to time is given as a factor of diameter (LS = $t.V/D$)

with the occurrence of puffs (Figs 6c and 7c), where the flow is mostly laminar with the occurrence of occasional puffs and fluctuations. The next stage, with a gradual increase in flow velocity, can be identified with the occurrence of slugs (Figs 6d and 7d) which can also be viewed as turbulent flow with some less intense regions. Some test cases also indicate the presence of both puffs and slugs, which can be considered as the stage before turbulence. Using these characteristics of intermittent structures as a criterion for identifying transition, the cases that undergo transition are shown in Table 2. From Table 2, going from S1 to S5, it is observed that the transition is pushed towards high flow rates, which is expected.

4.3 *Analysing transition*

After the qualitative observation of transition through the visualization of the transition structures, it is useful to analyse transition through statistical means and physical quantities to differentiate it with laminar and turbulent regimes. By such an approach, the identified cases of transition can be verified through other metrics. For this, (1) the intersection of the laminar and turbulent friction factor curves from the measured pressure drop is used mark the transition, and (2) the changes in turbulence intensity with respect to the increase in mean flow rate can also indicate transition.

Friction factor curves

Transition can be identified/verified from plotting the friction factor versus Reynolds number curves. Transition is assumed to occur at the intersection of the laminar and turbulent friction factor curves (Hedstrom, 1952). The Slatter Reynolds number is used here, as it considers both the shear-thinning behaviour of the fluid and the presence of yield stress. As a representative case, the friction factor curve for the case of slurry S5 (Fig. 9a) is plotted as it is the only case that contains enough measurements in the laminar flow regime. For the slurry, a number of pressure drop measurements were performed in the turbulent flow, however the UIV data were not retrieved for all of it, due to limitations of maximum detectable displacement mentioned in Section 3.3. Only the measurements that were resolvable are

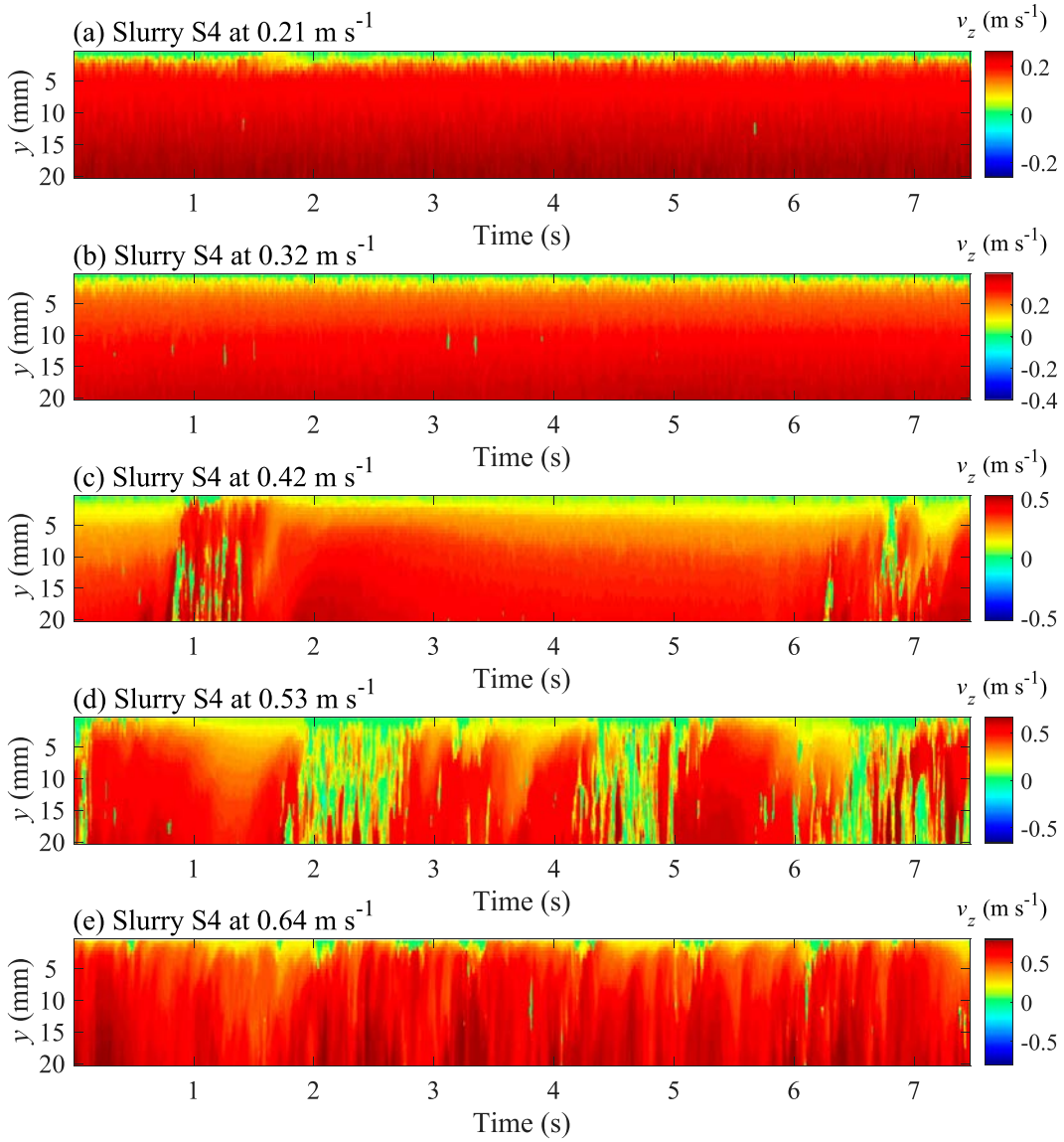

Figure 7 Observing transition through the ultrasound velocimetry data. Plot of the axial component of the velocity vector against time as an estimate for the cross-sectional plane for slurry S4

mentioned in Table 2. From Fig. 9, it can be seen that there is a sharp change in the data. Considering the lower $\mathsf{R_e}$ set of points before the sharp change to be laminar flow, and the higher $\mathsf{R_e}$ points as turbulent flow, the intersection of the extrapolated laminar and turbulent curves indicates the point of transition. Before further analysis, it is instructive to examine the friction factor curve. On plotting $f = 16/\mathsf{R_e}$, the laminar Fanning friction factor curve, it can be seen that the slurry measurements considered to be laminar fall on or close to the Fanning curve. But a striking result is obtained on plotting the Blasius turbulent curve. The Blasius curve is above the slurry measurements considered to be turbulent. This may be attributed to the use of the Slatter Reynolds number, as it is a particular representation of the viscous forces through rheology. To rule out any suspicion over measurement errors, the measured friction factor for the flow of water in the same set-up is plotted in the same figure. The friction factor curve for water falls right on the Blasius curve. The Slatter Reynolds number is used for water, it ultimately reduces to the standard Reynolds number as $\tau_y = 0$ and $n = 1$ for water for which the Blasius is valid. Furthermore, on comparing the measured wall shear-stress against analytical expressions for laminar and empirical expressions for turbulent flow from literature show that the errors from the measurement are not substantial. These results could certainly rule out measurement errors. To further analyse the discrepancy with respect to slurry S5, on plotting the friction factor versus Metzner–Reed Reynolds number (Fig. 9b) considering only the turbulent dataset of slurry S5, the data are shifted with respect to the data using the Slatter Reynolds number. This is to underline that the formulation of the Reynolds number for non-Newtonian fluids plays a huge role in discrepancies that arise. It must also be noted here that the friction factor curves are used merely to

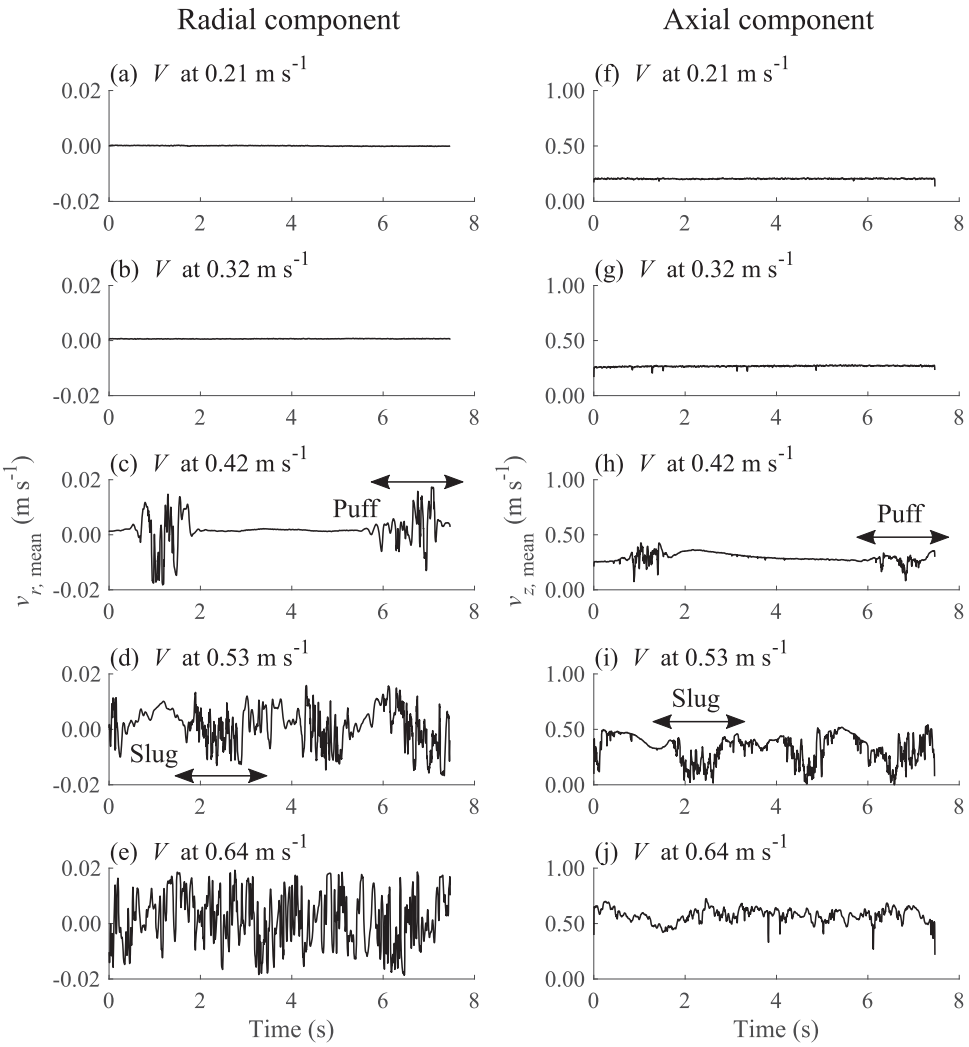

Figure 8 Plot of the mean of the velocity component along the radial direction against time. The radial component is used in figures (a), (b), (c), (d), (e) and the axial component in (f), (g), (h), (i), (j)

pinpoint the transition and not to analyse the friction losses in turbulence.

The observed point of transition for this slurry (S5, Table 2) is at 0.64 m s^{-1} (for this pipe diameter). There are no UIV data for slurry flow above this velocity due to the limitations of the equipment mentioned earlier (Section 3.3). On comparing the point of transition identified from the intersection of the friction factor curves with the one already observed for this slurry, it can be seen that the transition predicted at 0.64 m s^{-1} is close to the point of transition from the friction factor curves and lies on the extrapolated laminar curve. This observed point could be considered as one of the stages in the transition process.

Turbulence intensity

The occurrence of transition was further studied through the turbulence intensity, $I(= v'/V)$. As a representative case, Fig. 10 shows the turbulence intensity calculated using the time series of the velocity trace from the velocimetry versus mean flow velocity (from the flow meters) for slurry S4 using the velocity trace at 20 mm from the pipe wall. The turbulence intensity for the velocity component in the flow direction v_z when plotted against the mean axial velocity (Fig. 10) shows peaks at the same velocities where transitions were identified through the visualization of the flow field (Table 2). The sharp changes in peaks in turbulence intensities as a criterion for transition has also been used by Güzel, Burghelea, et al. (2009). On plotting the turbulence intensity for the v_r velocity component (Fig. 10), a steady increase in the turbulence intensity is seen on the onset of transition at about 0.32 m s^{-1}, and a sharp decrease at the onset of turbulence. Whereas, for the axial velocity component, the turbulence intensity increases gradually. Table 2 shows the measured cases of transition, which correspond to the data points where there is a sharp increase in turbulence velocity. These sharp changes in turbulence intensity for the radial velocity component that occur at the onset of transition is due to the definition of the turbulence intensity itself: it considers both the laminar parts of the velocity trace (low to no fluctuations) and the puffs and slugs (high fluctuations) in the calculation of v'. As the standard deviation between the laminar part and the part with the intermittent structures of the velocity trace has a large

Table 2 Identified flow regimes through the plotting of ultrasound velocimetry data and predictability of the transition models, S: Slatter, MR: Metzner–Reed and H: Hanks where the shading in green shows positive and red shows negative predictability. The Slatter and Metzner–Reed Reynolds numbers are provided for comparison.

V		S 1	S 2	S 3	S 4	S 5
0.21	Regime	Transition	Transition	Laminar	Laminar	Laminar
	Model	S MR H	S MR H	S MR H	S MR H	S MR H
	Re_S	13,058	11,567	7346	477	85
	Re_{MR}	12,865	11,150	6841	2005	1007
0.32	Regime	Turbulent	Turbulent	Transition	Laminar	Laminar
	Model	S MR H	S MR H	S MR H	S MR H	S MR H
	Re_S	20,408	18,776	12,703	1352	387
	Re_{MR}	20,106	18,099	11,829	3617	1879
0.42	Regime	Turbulent	Turbulent	Transition	Transition	Laminar
	Model	S MR H	S MR H	S MR H	S MR H	S MR H
	Re_S	27,226	25,669	18,090	2409	800
	Re_{MR}	26,824	24,744	16,846	5293	2811
0.53	Regime	Turbulent	Turbulent	Turbulent	Transition	Laminar
	Model	S MR H	S MR H	S MR H	S MR H	S MR H
	Re_S	34,839	33,543	24,478	3813	1400
	Re_{MR}	34,325	32,334	22,794	7330	3966
0.64	Regime	Turbulent	Turbulent	Turbulent	Turbulent	Transition
	Model	S MR H	S MR H	S MR H	S MR H	S MR H
	Re_S	42,549	41,667	31,279	5442	2120
	Re_{MR}	41,921	40,165	29,128	9545	5243

difference, the v' at transition has a high value. This in general tends to give a sharp change in the turbulence intensity at transition. Therefore, this can be considered as an intrinsic property of the velocity trace at transition.

It is concluded that the cases of transition that were identified using the visualization of the flow field from the UIV measurements correspond to the cases identified by other means (friction factor curve intersection, autocorrelation, turbulence intensity), which can be considered to be its verification.

4.4 *Predicting transition*

Cases of transition presented in Table 2 for the flow of slurry are the ones that were identified using the velocimetry plots and verified using other physical quantities mentioned in Section 4.3. From Section 1.2, three different transition predicting models are selected: the Slatter Reynolds number, Metzner–Reed Reynolds number and Hanks stability criterion. To apply the selected transition predicting models mentioned in Section 1.2, the transition velocity V_{trans} is used. The transition velocity is used as opposed to only Reynolds number, as the models used are varied and the transition velocity is common to all three of them. The rheology of the respective slurries (Table 1) is used to calculate these transition velocities. While the models predict only one transition velocity per slurry, the experimental measurements give us a range at which transition occurs as portrayed in Table 2.

Using the transition velocities, the flow regimes of each case and its predictability of the transition models is shown in Table 2. Table 2 shows the the flow regime at each flow velocity for each slurry studied. Further, the table also indicates whether the transition models are able to predict this flow regime as indicated with the aid of colours. Red indicates that the particular model was unable to predict the flow regime and green indicates that the model is very well able to predict the flow regime. Among the models studied here, the Reynolds number-based model by Slatter is very much capable of predicting the transition and flow regimes for fluids with yield stress and lower behaviour index (S4 and S5) as well as predicting the flow regimes of slurries that are only shear-thinning (S1, S2, S3). The second best is the stability parameter-based model of Hanks. That being said, on comparing the predicted transition velocity, both these models perform similarly. The error in predicting the median transition velocity of the Slatter model is 21% and of Hanks is 22% for slurries S4 and S5. Meanwhile, the error in predicting the median transition velocity for slurries S1, S2 and S3 is 76% for both models. The Metzner–Reed model performs with the lowest accuracy, with an error of 48% for slurries S4 and S5, and 78% for slurries S1, S2 and S3. It is observed that for slurries that are only shear-thinning (zero yield stress, slurries S1, S2, S3) all the models seem to fail in predicting the transition. The transition velocity predicted for these slurries is less than the ones measured; therefore, predicting a transition earlier than observed in reality. For slurries with a yield stress, the reason that the Slatter and Hanks model performed better could be that it uses the yield stress, while it is not incorporated in the Metzner–Reed model. For slurries that are only shear-thinning it is interesting to note that all the models predict more or less the same transition velocity. This could be attributed to

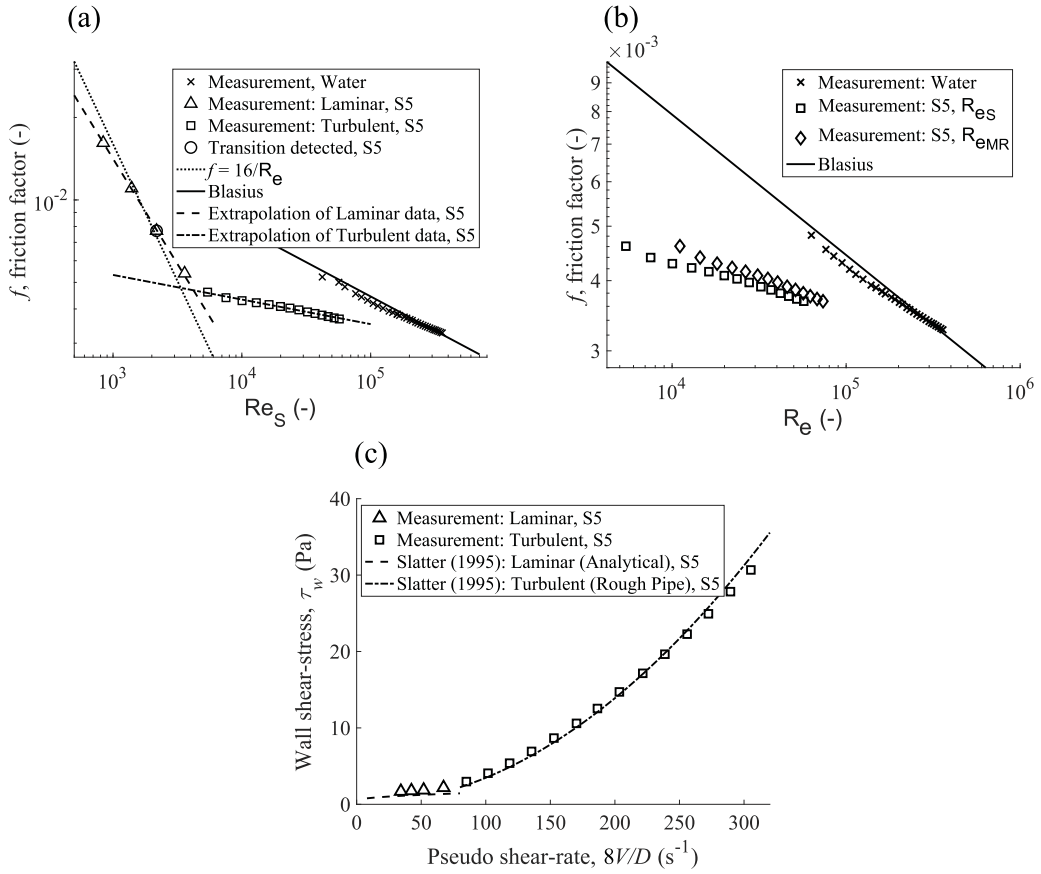

Figure 9 (a) Friction factor vs. Reynolds number curve for the flow of slurry S5. (b) Friction factor and Reynolds number for the turbulent dataset for slurry S5. (c) Comparing the measurements for slurry S5 obtained with laminar flow analytical expressions and turbulent flow empirical expressions from literature (Slatter, 1995)

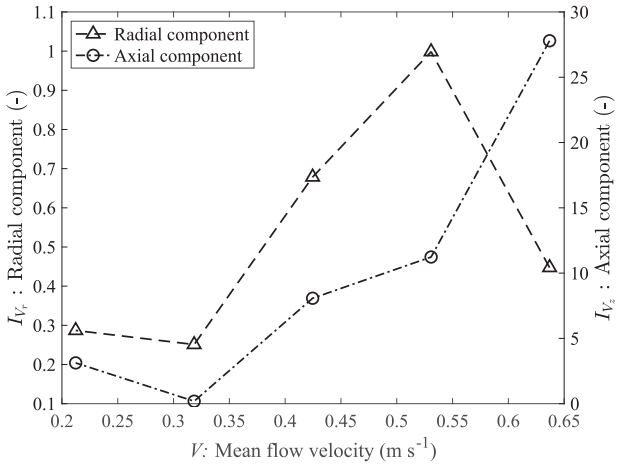

Figure 10 Plot of turbulence intensity using the velocity trace at 20 mm from the pipe wall for slurry S4 using both the radial and axial velocity component

the reduction of the Reynolds number-based models for weakly shear-thinning fluids to the standard Reynolds number and predict the same transition velocity. As for the Hanks models, this could also be true as the transition criteria used is similar to the Reynolds number-based models.

Therefore, it is concluded that the Slatter Reynolds number-based and Hanks stability parameter based model for fluids with a low behaviour index and yield stress has the capability to predict transition. The Slatter Reynolds number model has the advantage that it can easily be implemented compared to the stability parameter based models.

5 Conclusion and outlook

A test facility containing a pipe-loop was constructed to investigate and flow of non-Newtonian slurries and its transition from laminar to turbulent flow. To obtain images of the flow an ultrasound transducer was used. Using this imaging technique, it was demonstrated that UIV can be performed to obtain velocity measurements in slurry flows that are usually inaccessible to optical techniques. It is also demonstrated that using UIV measurements, it is also possible to obtain transition and turbulent statistics. UIV has also provided a new insight in transition through a novel visualization of the intermittent structures (puffs and slugs) that are formed during transition.

Transition was observed and identified through the visualization of the flow field with time. The cases wherein transition was observed were later verified by application of physical and statistical metrics. These verification metrics included intersection of the laminar and turbulent friction curves, autocorrelation of the flow field and turbulence intensity. These

verification metrics not only assisted in verifying the observed transition, but also in characterizing them. It is worth mentioning that the length of the intermittent structures are about five times the pipe diameter for the puffs and about 10 times the pipe diameter for the slugs. With the turbulent intensity, it is also seen that there is a sharp rise in its value upon transition. Through these, it is also concluded that transition occurs as a multistep process.

The transition velocity V_{trans} was used to access the models used to predict transition. Among them, the Reynolds number-based model of Slatter and the stability parameter based model of Hanks are assessed to be good in predicting transition for fluids with an yield stress and low behaviour index, while the one of Metzner–Reed is least favorable. The Slatter model also has an advantage in its ease of implementation.

Considering the promising results, the UIV technique has certainly a solid future in the field of multiphase flow studies, especially with its capability to be a non-intrusive diagnostic instrument and its applicability to optically inaccessible fluids. With the possibility to obtain longer time series and deeper intrusion (possibly a complete cross-section) in the pipe, its potential to investigate turbulence and transition is high. The realm of non-Newtonian fluids is still burgeoning. As most non-Newtonian fluids are opaque, the use of UIV could yield more understanding of turbulence and transition in flows, and hence provide a basis for improving CFD models for non-Newtonian fluids.

Acknowledgments

We would like to thank dr.ir. Sita Drost for her valuable time and effort in assisting in the UIV measurements.

Funding

This project is carried out by Delft University of Technology and funded by Technology Foundation STW, Deltares, Stowa, stichting RIONED, Waternet, Waterboard Zuiderzeeland, Sweco and XYLEM.

Supplemental data

Supplemental data for this article can be accessed https://doi.org/10.1080/00221686.2020.1770876.

Notation

A = cross-sectional area (m^2)
D = pipe diameter (m)
D_{shear} = diameter of the sheared region (m)
f = friction factor (–)
I = turbulence intensity (–)
K = fluid consistency index (Pa s^n)
L = length of pipe (m)
n = fluid behaviour index (–)
P = pressure (m)
Q = volumetric flow rate (m^3 s^{-1})
Q_{ann} = volumetric flow rate of the annular zone (m^3 s^{-1})
Q_{plug} = volumetric flow rate of the plug (m^3 s^{-1})
R = pipe radius (m)
R_{plug} = plug radius (m)
r = radial distance from the axis (m)
r_w = radial distance from the wall (m)
Re = Reynolds number (–)
$\mathrm{Re_{MR}}$ = Metzner–Reed Reynolds number (–)
$\mathrm{Re_S}$ = Slatter Reynolds number (–)
V = average flow velocity (m s^{-1})
V_{ann} = average flow velocity of the annular zone (m s^{-1})
V_{trans} = transition velocity (m s^{-1})
v = local velocity (m s^{-1})
v_r = velocity component along the radial direction (m s^{-1})
v_z = velocity component along the axial direction (m s^{-1})
v' = root mean square of the turbulent velocity fluctuations (m s^{-1})
y = distance from pipe wall, normal to axis (m)
Z = stability parameter (–)
Z_H = Hanks stability parameter (–)
Z_{RJ} = Ryan & Johnson stability parameter (–)
μ = fluid viscosity (Pa s)
ρ = fluid density (kg m^{-3})
τ = shear-stress (Pa)
τ_w = wall shear-stress (Pa)
τ_y = fluid yield stress (Pa)

ORCID

Jules van Lier http://orcid.org/0000-0003-2607-5425
Francois Clemens http://orcid.org/0000-0002-5731-0582

References

Avila, K., Moxey, D., de Lozar, A., Avila, M., Barkley, D., & Hof, B. (2011). *The onset of turbulence in pipe flow* (Vol. *33*). American Association for the Advancement of Science.

Bewersdorff, H.-W., & Thiel, H. (1993). Turbulence structure of dilute polymer and surfactant solutions in artificially roughened pipes. *Applied Scientific Research*, 50, 347–368. https://doi.org/10.1007/BF00850566.

Bogue, D. C. (1959). Entrance effects and prediction of turbulence in non-Newtonian flow. *Industrial & Engineering Chemistry*, *51*(7), 874–878. https://doi.org/10.1021/ie50595a044

Chen, R.-Y. (1973). Flow in the entrance region at low Reynolds numbers. *Journal of Fluids Engineering*, *95*(1), 153–158. https://doi.org/10.1115/1.3446948

Darbyshire, A. G., & Mullin, T. (1995). Transition to turbulence in constant-mass-flux pipe flow. *Journal of Fluid Mechanics*, *289*, 83–114. https://doi.org/10.1017/S0022112095001248

Draad, A. A., Kuiken, G. D. C., & Nieuwstadt, F. T. M. (1998). Laminar–turbulent transition in pipe flow for Newtonian and non-Newtonian fluids. *Journal of Fluid Mechanics*, *377*, 267–312. https://doi.org/10.1017/S0022112098003139

Durst, F., Ray, S., Ünsal, B., & Bayoumi, O. A. (2005). The development lengths of laminar pipe and channel flows. *Journal of Fluids Engineering*, *127*(6), 1154–1160. https://doi.org/10.1115/1.2063088

Eckhardt, B., Schneider, T. M., Hof, B., & Westerweel, J. (2007). Turbulence transition in pipe flow. *Annual Review of Fluid Mechanics*, *39*, 447–468. https://doi.org/10.1146/annurev.fluid.39.050905.110308

Escudier, M. P., & Presti, F. (1996). Pipe flow of a thixotropic liquid. *Journal of Non-newtonian Fluid Mechanics*, *62*(2-3), 291–306. https://doi.org/10.1016/0377-0257(96)01417-6

Eshtiaghi, N., Markis, F., & Slatter, P. (2012). The laminar/turbulent transition in a sludge pipeline. *Water Science and Technology*, *65*(4), 697–702. https://doi.org/10.2166/wst.2012.893

Froishteter, G. B., & Vinogradov, G. V. (1980). The laminar flow of plastic disperse systems in circular tubes. *Rheologica Acta*, *19*(2), 239–250. https://doi.org/10.1007/BF01521936

Güzel, B., Burghelea, T., Frigaard, I. A., & Martinez, D. M. (2009). Observation of laminar–turbulent transition of a yield stress fluid in Hagen–Poiseuille flow. *Journal of Fluid Mechanics*, *627*, 97–128. https://doi.org/10.1017/S0022112009005813

Güzel, B., Frigaard, I., & Martinez, D. M. (2009). Predicting laminar–turbulent transition in Poiseuille pipe flow for non-Newtonian fluids. *Chemical Engineering Science*, *64*(2), 254–264. https://doi.org/10.1016/j.ces.2008.10.011

Hanks, R. W. (1963). The laminar–turbulent transition for fluids with a yield stress. *AIChE Journal*, *9*(3), 306–309. https://doi.org/10.1002/(ISSN)1547-5905

Hanks, R. W. (1969). A theory of laminar flow stability. *AIChE Journal*, *15*(1), 25–28. https://doi.org/10.1002/(ISSN)1547-5905

Hanks, R. W., & Dadia, B. H. (1971). Theoretical analysis of the turbulent flow of non-Newtonian slurries in pipes. *AIChE Journal*, *17*(3), 554–557. https://doi.org/10.1002/(ISSN)1547-5905

Hanks, R. W., & Ricks, B. L. (1974). Laminar-turbulent transition in flow of pseudoplastic fluids with yield stresses. *Journal of Hydronautics*, *8*(4), 163–166. https://doi.org/10.2514/3.62992

Hedstrom, B. O. A. (1952). Flow of plastic materials in pipes. *Industrial & Engineering Chemistry*, *44*(3), 651–656. https://doi.org/10.1021/ie50507a056

Hof, B., Juel, A., & Mullin, T. (2003). Scaling of the turbulence transition threshold in a pipe. *Physical Review Letters*, *91*(24), 244502. https://doi.org/10.1103/PhysRevLett.91.244502

Hogendoorn, W., & Poelma, C. (2018). Particle-laden pipe flows at high volume fractions show transition without puffs. *Physical Review Letters*, *121*(19), 194501. https://doi.org/10.1103/PhysRevLett.121.194501

Kelessidis, V. C., Maglione, R., Tsamantaki, C., & Aspirtakis, Y. (2006). Optimal determination of rheological parameters for Herschel–Bulkley drilling fluids and impact on pressure drop, velocity profiles and penetration rates during drilling. *Journal of Petroleum Science and Engineering*, *53*(3-4), 203–224. https://doi.org/10.1016/j.petrol.2006.06.004

Lindgren, E. R. (1969). Propagation velocity of turbulent slugs and streaks in transition pipe flow. *The Physics of Fluids*, *12*(2), 418–425. https://doi.org/10.1063/1.1692497

Masalova, I., Malkin, A. Y., Kharatiyan, E., & Haldenwang, R. (2006). Scaling in pipeline flow of kaolin suspensions. *Journal of Non-newtonian Fluid Mechanics*, *136*(1), 76–78. https://doi.org/10.1016/j.jnnfm.2006.03.002

Metzner, A. B., & Reed, J. C. (1955). Flow of non-newtonian fluids-correlation of the laminar, transition, and turbulent-flow regions. *AIChE Journal*, *1*(4), 434–440. https://doi.org/10.1002/(ISSN)1547-5905

Mishra, P., & Tripathi, G. (1971). Transition from laminar to turbulent flow of purely viscous non-Newtonian fluids in tubes. *Chemical Engineering Science*, *26*(6), 915–921. https://doi.org/10.1016/0009-2509(71)83051-8

Nishi, M., Ünsal, B., Durst, F., & Biswas, G. (2008). Laminar-to-turbulent transition of pipe flows through puffs and slugs. *Journal of Fluid Mechanics*, *614*, 425–446. https://doi.org/10.1017/S0022112008003315

Peixinho, J., Nouar, C., Desaubry, C., & Théron, B. (2005). Laminar transitional and turbulent flow of yield stress fluid in a pipe. *Journal of Non-Newtonian Fluid Mechanics*, *128*(2-3), 172–184. https://doi.org/10.1016/j.jnnfm.2005.03.008

Poelma, C. (2017). Ultrasound imaging velocimetry: A review. *Experiments in Fluids*, *58*(1), 3. https://doi.org/10.1007/s00348-016-2283-9

Poelma, C., Van der Mijle, R. M. E., Mari, J. M., Tang, M.-X., Weinberg, P. D., & Westerweel, J. (2012). Ultrasound imaging velocimetry: Toward reliable wall shear stress measurements. *European Journal of Mechanics - B/Fluids*, *35*, 70–75. https://doi.org/10.1016/j.euromechflu.2012.03.003

Poole, R. J., & Ridley, B. S. (2007). Development-length requirements for fully developed laminar pipe flow of inelastic non-Newtonian liquids. *Journal of Fluids Engineering*, *129*(10), 1281–1287. https://doi.org/10.1115/1.2776969

Ryan, N. W., & Johnson, M. M. (1959). Transistion from laminar to turbulent flow in pipes. *AIChE Journal*, *5*(4), 433–435. https://doi.org/10.1002/(ISSN)1547-5905

Singh, J., Rudman, M., Blackburn, H. M., Chryss, A., Pullum, L., & Graham, L. J. W. (2016). The importance of rheology characterization in predicting turbulent pipe

flow of generalized newtonian fluids. *Journal of Non-Newtonian Fluid Mechanics*, *232*, 11–21. https://doi.org/10.1016/j.jnnfm.2016.03.013

Slatter, P. T. (1995). *Transitional and turbulent flow of non-Newtonian slurries in pipes* [Doctoral dissertation]. University of Cape Town.

Soto, R. J., & Shah, V. L. (1976). Entrance flow of a yield-power law fluid. *Applied Scientific Research*, *32*(1), 73–85. https://doi.org/10.1007/BF00540777

Thota Radhakrishnan, A. K., van Lier, J. B., & Clemens, F. H. L. R. (2018). Rheological characterisation of concentrated domestic slurry. *Water Research*, *141*:235–250. https://doi.org/10.1016/j.watres.2018.04.064

Van Doorne, C. W. H., & Westerweel, J. (2007). Measurement of laminar, transitional and turbulent pipe flow using stereoscopic-PIV. *Experiments in Fluids*, *42*(2):259–279. https://doi.org/10.1007/s00348-006-0235-5

Wygnanski, I., Sokolov, M., & Friedman, D. (1975). On transition in a pipe. Part 2. The equilibrium puff. *Journal of Fluid Mechanics*, *69*(2), 283–304. https://doi.org/10.1017/S0022112075001449

Wygnanski, I. J., & Champagne, F. H. (1973). On transition in a pipe. Part 1. The origin of puffs and slugs and the flow in a turbulent slug. *Journal of Fluid Mechanics*, *59*(2), 281–335. https://doi.org/10.1017/S0022112073001576